Journal of Solid State Chemistry **155,** 78–85 (2000)
doi:10.1006/jssc.2000.8894, available online at http://www.idealibrary.com on IDEAL®

Phase Equilibria and Dielectric Behavior in the $CaO:Al_2O_3:Nb_2O_5$ System

T. A. Vanderah,* W. Febo,† Julia Y. Chan,* R. S. Roth,* J. M. Loezos,* L. D. Rotter,* R. G. Geyer,‡ and D. B. Minor*

**Materials Science and Engineering Laboratory, National Institute of Standards and Technology, Gaithersburg, Maryland 20899; †University of Puerto Rico, Cayey Campus, Cayey, Puerto Rico 00736; and ‡Electronics and Electrical Engineering Laboratory, National Institute of Standards and Technology, Boulder, Colorado 80303*

Received June 14, 2000; accepted July 27, 2000

DEDICATED TO PROFESSOR J. M. HONIG

Subsolidus phase equilibria in the $CaO:Al_2O_3:Nb_2O_5$ system at 1325°C in air have been determined. One ternary phase forms, Ca_2AlNbO_6, which exhibits a perovskite-related structure with 1:1 or NaCl-type ordering of Al^{3+} and Nb^{5+} on the *B* sites. Indexed X-ray powder diffraction data for this monoclinic compound are given ($P2_1/n$ (No. 11); $a = 5.3780(1)$, $b = 5.4154(1)$, $c = 7.6248(2)$ Å, $\beta = 89.968(2)°$). The subsystem $CaO–Nb_2O_5$ was reexamined at CaO contents above 70 mol% to clarify inconsistencies in the literature. Two phases were confirmed to form in this region: the polymorphic-ordered perovskite $Ca_4Nb_2O_9$, with solid solution ranging from approximately 17 to 20.5 mol% Nb_2O_5, and the compound referred to as $Ca_3Nb_2O_8$, which was shown here to occur as essentially a point compound at the composition 75.25:24.75 $CaO:Nb_2O_5$. The perovskite-related structure of the $Ca_3Nb_2O_8$-type phase was shown to be noncubic, and further studies are in progress. Capacitance methods at 1 MHz were used to determine the dielectric constants and associated temperature coefficients for eleven compounds in the $CaO:Al_2O_3:Nb_2O_5$ system. Ca_2AlNbO_6 and $Ca_3Nb_2O_8$ coexist in equilibria and were found to exhibit temperature coefficients of permittivity with opposite signs. Five compositions in the xCa_2AlNbO_6:$(1-x)Ca_3Nb_2O_8$ system were prepared and their dielectric properties measured by dielectric resonator methods at 5–7 GHz. The relative permittivities and temperature coefficients of resonant frequency obtained for the endmembers Ca_2AlNbO_6 and $Ca_3Nb_2O_8$ were 30, −88 ppm/°C, and 45, +113 ppm/°C, respectively. Temperature compensation of the resonant frequency was obtained near $x = 0.67$ with a permittivity of 32; no solid solution was detected by X-ray powder diffraction.

Key Words: **$CaO:Al_2O_3:Nb_2O_5$, xCa_2AlNbO_6:$(1-x)Ca_3Nb_2O_8$; Ca_2AlNbO_6; $Ca_3Nb_2O_8$; $Ca_4Nb_2O_9$; $CaO:Nb_2O_5$; microwave dielectric properties; phase diagram; calcium aluminum niobates; calcium niobates.**

INTRODUCTION

Dielectric oxide ceramics with high permittivity, low dielectric loss, and near-zero temperature dependence of dielectric constant are critical elements in components such as resonators, oscillators, and filters for wireless communications (1–4). Relatively few ceramic systems are currently available with the properties needed for practical applications at various operating frequencies (5). Tantalate-based perovskite derivatives $Ba_3MTa_2O_9$, with M = Zn or Mg (5–8), are unique in exhibiting permittivities of about 30 together with extremely low dielectric loss tangents ($< 10^{-5}$ at 1 GHz). The present work was motivated by the need for dielectric oxides that could serve as less costly alternatives to the tantalate systems for high-frequency, high-power resonator applications. Ternary Al_2O_3–Nb_2O_5-containing systems were selected for study (9) because the polarizability of Ta^{5+} is intermediate[1] between that of Al^{3+} and Nb^{5+}, and because similar crystal chemistry is expected. The present report describes a systematic study of the subsolidus phase equilibria relations and dielectric properties in the $CaO–Al_2O_3–Nb_2O_5$ system.

Review of Prior Work

The $CaO–Al_2O_3$ system has been well studied owing to its importance in structural ceramic materials (15); five binary compounds are known to form: $Ca_3Al_2O_6$, $Ca_{12}Al_{14}O_{33}$ (moisture-sensitive), $CaAl_2O_4$, $CaAl_4O_7$, and $CaAl_{12}O_{19}$ (16).

In several studies of the binary Al_2O_3–Nb_2O_5 system (15), compounds have been reported to occur at molar ratios of 1:1, 1:9, 1:11, 1:25, and 1:49, respectively. However, the preponderance of experimental evidence suggests that only three binary compounds form at 1:1, 1:11, and 1:49 (9, 17–22).

[1]Although the polarizability of Ta^{5+} given in (10) (4.73 Å^3) is larger than that given for Nb^{5+} (3.97 Å^3), considerable experimental data suggest that the reverse is true (11, 12). For example, the relative permittivities of isostructural $Ba_3ZnTa_2O_9$ and $Ba_3ZnNb_2O_9$ are ~30 (5) and ~40 (13), respectively. Similarly, for Ca_2AlNbO_6 and Ca_2AlTaO_6 the respective values are 25 and 20 (14).

0022-4596/00 $35.00

The $CaO–Nb_2O_5$ binary system has been the least studied with some variability in reported results (15). Three equilibrium phases, $Ca_3Nb_2O_8$, $Ca_2Nb_2O_7$, and $CaNb_2O_6$, were indicated in the earliest published phase diagram (23). A later study (24) indicated $Ca_2Nb_2O_7$ and $CaNb_2O_6$ as equilibrium phases, in addition to three "$Ca_4Nb_2O_9$-type" solid solution phases; the authors did not report the existence of $Ca_3Nb_2O_8$. $Ca_2Nb_2O_7$ and $CaNb_2O_6$ have been well characterized; the former occurs with a monoclinic perovskite-slab-type structure (25–27), and the latter adopts a columbite-type structure (28–30). The polymorphic perovskite derivative $Ca_4Nb_2O_9$ has recently been characterized in detail (31, 32). This compound exhibits four structures with different Ca and Nb ordering on the *B*-cation sites. The phases include a low-temperature 2:1 ordering ($T < 1400°C$), a metastable "3:1" ordering ($T < 1400°C$), and two high-temperature forms with 1:1 NaCl-like ordering ($T > 1400°C$). The highest-temperature polymorph without octahedral tilting can only be distinguished by a change in microstructure of specimens quenched from $T > 1500°C$.

Reports describing the compound $Ca_3Nb_2O_8$ are variable. Initially, this phase was reported as an incongruently melting (1560°C) perovskite derivative with two polymorphs, referred to as cubic "Type I" and a "Type II" (23). The authors indexed the X-ray powder pattern for Type I with a unit cell of $a = 23.934$ Å, and stated that "it satisfies the vast majority of the faint lines" (23). Subsequent work from the same laboratory showed that Type II was actually one of the $Ca_4Nb_2O_9$ polymorphs, and reported a phase diagram that does not contain $Ca_3Nb_2O_8$ (24). Later studies using electron and X-ray diffraction concluded that $Ca_3Nb_2O_8$ forms with a tetragonal perovskite-related cell ($a = 16.90$ Å $\approx 3\sqrt{2}a_c$, $c = 23.73$ Å $\approx 6a_c$, $P4/nnc$, where $a_c = 4$ Å for cubic perovskite) (33); however, these authors concluded that the phase is oxygen deficient, i.e., $Ca_3Nb_2O_{8-x}$. An X-ray powder diffraction pattern was given (33) with indices based on this tetragonal cell, which accounted for observed peaks not allowed by the cubic 23.934-Å cell reported earlier (23).

The ternary compound Ca_2AlNbO_6 was described in 1965 (34) as a perovskite derivative with an orthorhombic superstructure ($a = 5.38$ Å $\approx \sqrt{2}a_c$, $b = 5.40$ Å $\approx \sqrt{2}a_c$, $c = 7.61$ Å $\approx 2a_c$; X-ray powder data) arising from ordering of Al^{3+} and Nb^{5+} on the octahedral *B* sites. Ca_2AlNbO_6 reportedly melts congruently at 1675°C (35), and its dielectric behavior has been characterized at gigahertz frequencies ($\varepsilon_r = 25$, $Qxf = 7500$ GHz, $\tau_f = -87$ ppm/°C) (14). The structure of Ca_2AlNbO_6 is illustrated in Fig. 1. The arrangement is very similar to that in $CaTiO_3$ (36), with 1:1 or NaCl-like ordering of Al^{3+} and Nb^{5+} superimposed on octahedral tilting.

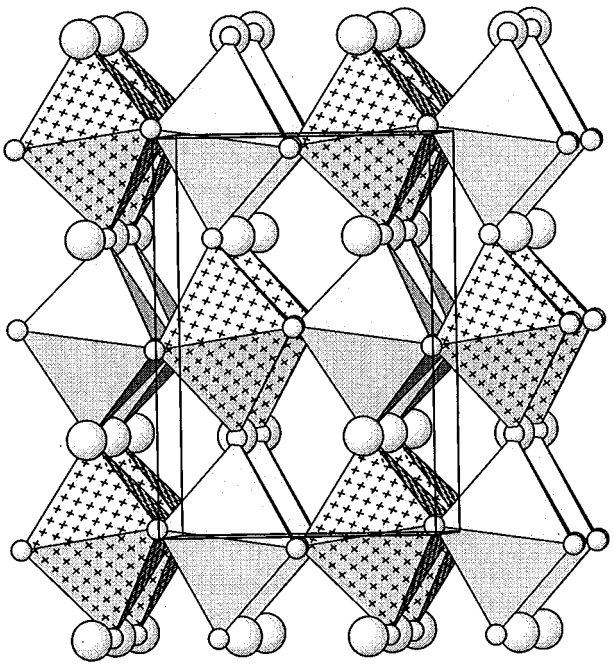

FIG. 1. The structure of the perovskite derivative Ca_2AlNbO_6. Large spheres denote Ca^{2+}, small spheres, oxygen; stippled and gray octahedra represent the 1:1 or NaCl-like ordered Al^{3+} and Nb^{5+} sites. The arrangement is very similar to that in $CaTiO_3$, with a slight monoclinic distortion (36).

EXPERIMENTAL METHODS

Specimens were prepared by solid-state reaction of $CaCO_3$ (99.999%), Al_2O_3 (0.3 μm, 99.99%) and Nb_2O_5 (optical grade). Prior to each heat treatment, samples were ground with an agate mortar and pestle for 15 min, pelletized, and placed on sacrificial powder of the same composition in a Pt-foil-lined alumina combustion boat. After an initial overnight calcine at 950°C, multiple 2–4 day heatings (with intermediate grinding and repelletizing) were carried out in the temperature range 1300–1400°C, 25–50°C below the solidus temperatures that had been previously determined by melting point experiments; samples were furnace-cooled to ~750°C and then air-quenched on the benchtop. The minimum solidus temperature observed in the ternary system was ~1350°C, for the composition 0.20:0.20:0.60 $CaO:Al_2O_3:Nb_2O_5$. Typically, three to six heatings were required to attain equilibrium, which was presumed when no further changes could be detected in the weakest peaks observed in the X-ray powder diffraction patterns. Phase relations determined in this manner were reconfirmed by annealing specimens at 1325°C followed by water quenching. Quenching, melting point, and crystal-growth experiments were carried out in sealed Pt capsules. The colors of the polycrystalline specimens ranged from white to light tan. Single crystals of the $Ca_3Nb_2O_8$-type phase were grown from a flux of $3CaO:V_2O_5$ at a 50:50 wt.% mixture of equilibrated $Ca_3Nb_2O_8$ powder and flux.

The mixture was annealed for 2 h at 1475°C, cooled at 1°C/h to 1300°C, and removed from the furnace. Pale yellow crystals exhibiting glassy fracture were harvested from the reaction mass by leaching with dilute hydrochloric acid. Attempts to grow crystals of $Ca_3Nb_2O_8$ using neat charges slow-cooled from 1575°C were not successful, nor were experiments carried out at 1200°C using NaCl as a flux.

Phase assemblages were ascertained from X-ray powder diffraction data, which were obtained with a Philips[2] diffractometer equipped with incident Soller slits, θ-compensating slit, a graphite monochromator, and a scintillation detector. Samples were mounted in welled glass slides. Routine identification patterns were collected at ambient temperatures using Cu$K\alpha$ radiation with a 0.02° 2θ step size and a 2-s count time. For Ca_2AlNbO_6, a longer scan was taken (0.010° 2θ step size, 5 s count time) to obtain data for least-squares refinement of lattice parameters. Intensity data (measured as relative peak heights above background) of hand-picked peaks were obtained using the Siemens DIFFRAC5000 second-derivative peak locate program. The observed 2θ line positions reported here for Ca_2AlNbO_6 have been corrected using SRM 660, LaB_6 (37) as an external calibrant. Lattice parameters were refined using the corrected powder diffraction data (2θ values, Cu$K\alpha_1 = 1.540562$ Å) with the least-squares progam CELLSVD (38). During the refinement, the indices of unequivocally indexed reflections were fixed in accordance with the powder pattern calculated using the GSAS package (39) and the positional parameters reported by Levin *et al.*, from a neutron powder diffraction study of the Ca_2AlNbO_6–$CaTiO_3$ system (36). For the $Ca_3Nb_2O_8$-type phase, high-resolution X-ray powder data were collected using a Siemens D5000 diffractometer equipped with a focusing Ge incident beam monochromator, a sample spinner, and a scanning position-sensitive detector (PSD). The scan range was from 15° to 155° 2θ. Single crystals were characterized by the precession camera method using Zr-filtered Mo$K\alpha$ radiation.

Dielectric properties were evaluated by capacitance methods at 1 MHz using cylindrical pellets (diameters 8–9 mm) pressed from equilibrated powders, sintered $\sim$ 50°C below the solidus temperatures, and then polished to a height of approximately 1.5 mm. Sample density (ρ_{obs}) was estimated from the mass and dimensions of the pellets and compared to the crystallographic density (ρ_{calc}) to estimate pore volume. Electrodes were formed by thermally evaporating approximately 25 nm of Cr followed by 300 nm of Au onto an 8.0-mm circular area on the cylinder faces in order to form parallel plate capacitors. Au wires were attached to each electrode and to Pt wires leading to an HP4194A Impedance Analyzer. All contacts were made with Ag paint. Variable-temperature data were obtained by heating the capacitors in a box furnace; specimen temperature was measured by a case-grounded K-type thermocouple located under the capacitor. The lead-compensated capacitance was measured with the impedance analyzer in the frequency range 100 Hz to 10 MHz, with an oscillator amplitude of 0.5 V, while the temperature decreased from 200 to 25°C over $\sim$ 15 h, with the furnace power off. The capacitance at 25°C and its temperature coefficient were determined from a linear regression of the 1-MHz data taken over the range 25 to 100°C. Both quantities were corrected for edge effects (40) and used to calculate the observed dielectric constant ε_{obs} and its temperature coefficient, which were then corrected for porosity using the Bruggeman effective medium theory (41) to give ε_{corr} and τ_ε. The uncertainty in the dielectic constants and their temperature coefficients is $\pm 20\%$ and is mainly attributed to imprecise overlap of the electrodes on each side of the capacitor.

The dielectric properties of five specimens along the composition line Ca_2AlNbO_6–$Ca_3Nb_2O_8$ were evaluated at microwave frequencies (5–8 GHz) using cylindrical pellets (diameters and heights 8–9 mm) that has been pressed from equilibrated powders, sintered at 1475°, and polished. Samples were measured as TE_{011} or $TE_{0\gamma\delta}$ dielectric resonators in a parallel plate waveguide using the Hakki–Coleman or Courtney (42, 43), or modified Courtney (44, 45) techniques. Variable-temperature data were obtained at six temperatures between 20 and 100°C using the specimen as a TE_{011} dielectric resonator situated internally in a cylindrical cavity. Relative real permittivity (ε_r') was calculated from the measured frequency of the TE_{011} or $TE_{0\gamma\delta}$ resonance mode and sample dimensions; loss tangent ($\tan\delta$) was determined from the measured system unloaded Q factor. For all results reported, variable-temperature and variable-frequency conductor losses were measured and accounted for. The temperature coefficient of resonant frequency (τ_f) was calculated from a linear regression analysis of the data obtained at different temperatures. The quality factor Q was calculated as $(\tan\delta)^{-1}$. Permittivity and dielectric loss tangent values were corrected to theoretical density using effective-medium theory (46, 47). The uncertainties in the reported permittivity values are approximately $\pm 10\%$, and are dominated by the estimate of pore volume. The estimated uncertainty in measurement of loss tangent is 2×10^{-5}.

RESULTS AND DISCUSSION

CaO:Al_2O_3:Nb_2O_5 System

The subsolidus phase equilibria relations found in the present study are shown in Fig. 2 along with the dielectric constant, and the sign of its temperature dependence, for selected compounds. Only one ternary compound,

[2]Certain commercial equipment is identified in order to adequately specify the experimental procedure; recommendation or endorsement by the National Institute of Standards and Technology is not therein implied.

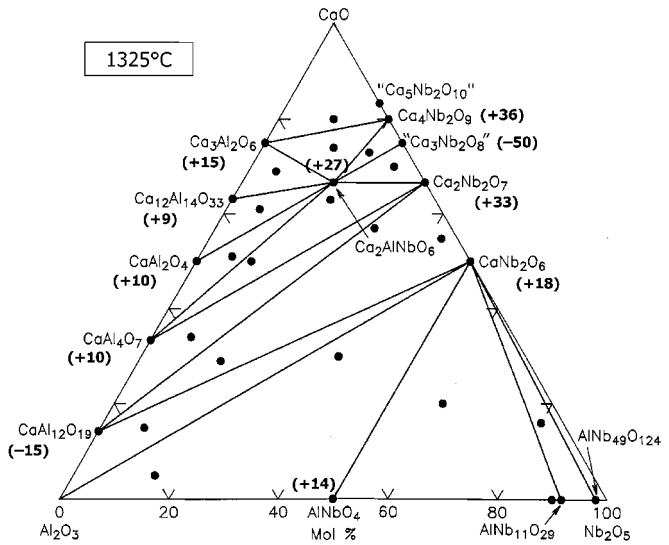

FIG. 2. Subsolidus phase equilibria relations found in the $CaO:Al_2O_3:Nb_2O_5$ system in air. The dielectric constants (ε_{corr}) and the signs of their temperature dependences (τ_ε) are included for selected compounds (Table 2). Ca_2AlNbO_6 and $Ca_3Nb_2O_8$ occur in equilibrium with each other and exhibit opposite signs of τ_ε.

Ca_2AlNbO_6, was found to occur. Powder diffraction data for this compound are given in Table 1 and have been indexed on the basis of a monoclinic unit cell ($P2_1/n$ (No.11); $a = 5.3780(1)$, $b = 5.4154(1)$, $c = 7.6248(2)$ Å, $\beta = 89.968(2)^\circ$) (36), which is very similar to the $CaTiO_3$-like orthorhombic cell reported in earlier work (34).

In contrast to the analogous systems $SrO:Al_2O_3:Nb_2O_5$ (9) and $BaO:Al_2O_3:Nb_2O_5$ (49), the tetragonal tungsten bronze (TTB) structure was not observed to form in the CaO-containing ternary: a specimen with nominal composition $Ca_6AlNb_9O_{30}$, equilibrated within 20°C of the solidus (1425°C), yielded a 3-phase mixture of $Ca_2Nb_2O_7$, $CaNb_2O_6$, and $CaAl_{12}O_{19}$. This observation is consistent with the narrow region of stability of the TTB structure in the $SrO:Al_2O_3:Nb_2O_5$ system—the structure is destabilized upon proceeding to the smaller Ca^{2+} ion. In the present study, X-ray powder diffraction data indicated no evidence of solid solution formation around the compound $AlNbO_4$, as was reported in a study of the $MgO:Al_2O_3:Nb_2O_5$ system (50).

The observed and corrected dielectric constants (ε_{obs} and ε_{corr}) and their corrected temperature coefficients (τ_ε) for selected compositions in the $CaO:Al_2O_3:Nb_2O_5$ system are given in Table 2. Positive temperature coefficients of permittivity were observed for most of the compositions, while negative values were obtained for $CaAl_{12}O_{19}$ and $Ca_3Nb_2O_8$. The $Ca_4Nb_2O_9$ sample was a mixture of polymorphic forms, which are known to exhibit differences in dielectric properties (32). The temperature dependence of the permittivity of Ca_2AlNbO_6 is opposite in sign and similar in magnitude to that of $Ca_3Nb_2O_8$, as shown in

TABLE 1
X-Ray Powder Diffraction Data for Ca_2AlNbO_6

h	k	l	$2\theta_{obs}$	I_{obs}	$2\theta_{calc}$	$\Delta 2\theta$	d_{obs}
0	1	1	20.101	14	20.095	0.006	4.4138
1	0	1			20.184		
−1	0	1			20.194		
1	1	0			23.291		
0	0	2	23.303	18	23.313	−0.010	3.8140
1	1	1	26.075	1	26.087	−0.012	3.4145
0	2	0	33.033	47	33.055	−0.022	2.7094
1	1	2			33.183		
−1	1	2	33.192	100	33.196	−0.004	2.6968
2	0	0	33.277	41	33.292	−0.015	2.6901
0	2	1	35.128	1	35.141	−0.013	2.5525
1	2	0	37.144	1	37.144	0.000	2.4184
2	1	0	37.300	1	37.305	−0.005	2.4087
1	0	3	39.167	18	39.162	0.005	2.2981
0	2	2	40.834	2	40.843	−0.009	2.2080
1	1	3	42.709	1	42.701	0.008	2.1153
−1	2	2	44.332	1	44.323	0.009	2.0416
2	2	0	47.634	72	47.621	0.013	1.9075
0	0	4			47.668		
2	2	1	49.163	2	49.180	−0.017	1.8516
1	2	3	52.161	7	52.156	0.005	1.7521
−2	1	3	52.301	6	52.300	0.001	1.7477
3	0	1			52.380		
1	3	0	53.516	6	53.502	0.014	1.7108
2	2	2			53.664		
−2	2	2	53.679	10	53.683	−0.004	1.7060
1	1	4			53.697		
−1	1	4			53.715		
1	3	1	54.930	2	54.941	−0.011	1.6701
−3	1	1	55.273	1	55.266	0.007	1.6605
1	3	2			59.121		
−1	3	2	59.153	33	59.130	0.023	1.5605
3	1	2	59.414	41	59.415	−0.001	1.5543
−3	1	2			59.440		
2	1	4	62.025	1	62.024	0.001	1.4950
2	3	1	63.185	3	63.169	0.016	1.4703
−1	0	5	63.352	5	63.350	0.002	1.4668
1	3	3	65.708	1	65.720	−0.012	1.4198
1	1	5	65.904	1	65.896	0.008	1.4161
0	4	0	69.360	8	69.355	0.005	1.3537
2	2	4			69.653		
−2	2	4	69.671	28	69.684	−0.013	1.3484
4	0	0	69.882	9	69.908	−0.026	1.3449
0	4	1	70.577	1	70.599	−0.022	1.3333
1	4	0	71.832	1	71.847	−0.015	1.3131
4	1	0	72.380	1	72.358	0.022	1.3045
−1	4	1	73.088	2	73.075	0.013	1.2936
−1	2	5	73.333	4	73.341	−0.008	1.2899
−2	1	5	73.477	5	73.452	0.025	1.2877
4	1	1	73.579	3	73.573	0.006	1.2862
0	4	2	74.279	2	74.280	−0.001	1.2758
1	3	4	74.435	3	74.434	0.001	1.2735
−1	3	4			74.449		
3	1	4	74.676	2	74.688	−0.012	1.2700
−3	3	1	75.778	1	75.756	0.022	1.2542
−4	1	2	77.212	1	77.222	−0.010	1.2345
2	4	0	79.138	7	79.137	0.001	1.2092
3	3	2			79.332		
−3	3	2	79.371	18	79.355	0.016	1.2062

TABLE 1— *Continued*

h	k	l	$2\theta_{obs}$	I_{obs}	$2\theta_{calc}$	$\Delta 2\theta$	d_{obs}
4	2	0	79.530	9	79.532	−0.002	1.2042
0	4	3	80.297	1	80.277	0.020	1.1946
2	2	5	80.564	1	80.557	0.007	1.1913
−1	4	3	82.672	1	82.660	0.012	1.1662
−4	1	3	83.180	1	83.166	0.014	1.1604
2	4	2	83.840	1	83.860	−0.020	1.1529
4	2	2	84.240	1	84.244	−0.004	1.1485
−1	3	5	85.181	1	85.161	0.020	1.1382
−3	1	5	85.430	1	85.439	−0.009	1.1355
0	4	4	88.493	6	88.510	−0.017	1.1039
4	0	4			88.999		
−4	0	4	89.041	3	89.058	−0.017	1.0985
−1	0	7	92.378	2	92.372	0.006	1.0674
5	0	1	92.628	1	92.635	−0.007	1.0652
3	3	4	93.436	1	93.418	0.018	1.0581
5	1	0	93.776	1	93.795	−0.019	1.0551
1	5	1	94.162	1	94.186	−0.024	1.0518
3	4	2	95.631	1	95.632	−0.001	1.0395
1	5	2	97.693	5	97.712	−0.019	1.0230
1	3	6	98.019	5	98.037	−0.018	1.0204
−3	1	6	98.332	12	98.343	−0.011	1.0180
−5	1	2	98.526	7	98.520	0.006	1.0165
0	5	3	101.257	1	101.262	−0.005	0.9964
2	1	7	101.791	2	101.787	0.004	0.9926
4	1	5	101.911	2	101.921	−0.010	0.9917
1	5	3	103.648	1	103.664	−0.016	0.9798
4	4	0	107.710	3	107.691	0.019	0.9538
4	4	1	108.922	1	108.915	0.007	0.9466
1	5	4	112.282	1	112.276	0.006	0.9275
−1	5	4			112.292		
4	4	2			112.660		
−4	4	2	112.716	1	112.692	0.024	0.9252
0	6	0	117.160	1	117.173	−0.013	0.9026
3	5	2	117.538	6	117.536	0.002	0.9008
−3	5	2			117.560		
−3	3	6	117.968	7	117.957	0.011	0.8987
1	6	1	121.191	1	121.205	−0.014	0.8841
−2	3	7	121.949	1	121.930	0.019	0.8809
6	1	1	122.512	1	122.529	−0.017	0.8785
2	4	6	123.081	1	123.089	−0.008	0.8761
4	2	6	123.550	1	123.528	0.022	0.8742
1	5	5	124.235	1	124.245	−0.010	0.8714
2	6	0	128.370	2	128.375	−0.005	0.8556
4	4	4			129.046		
−4	4	4	129.137	8	129.122	0.015	0.8529
2	2	8			129.180		
−2	2	8			129.256		
6	2	0	129.730	2	129.710	0.020	0.8508
1	4	7	133.503	1	133.501	0.002	0.8383
−6	1	3	134.553	6	134.570	−0.017	0.8351
3	5	4			134.995		
−3	5	4	135.080	1	135.057	0.023	0.8335
3	1	8	135.676	1	135.665	0.011	0.8317

Note. $P2_1/n$ (No. 11); $a = 5.3780(1)$, $b = 5.4154(1)$, $c = 7.6248(2)$ Å; $\beta = 89.968(2)^\circ$ (Figure of merit (48): $F(90) = 18.7(0.0116, 414)$).

Fig. 3. Since these compounds were found to occur in equilibrium with each other (Fig. 2), a temperature-compensated, thermodynamically stable mixture was expected to form on the Ca_2AlNbO_6–$Ca_3Nb_2O_8$ join.

Five specimens were prepared in the xCa_2AlNbO_6:$(1-x)$ $Ca_3Nb_2O_8$ system with x values 0.0, 0.25, 0.50, 0.75, and 1.0. No solid solution formation was detectable by X-ray powder diffraction. The dielectric properties obtained for these compositions at microwave frequencies are given in Table 3. Figure 4 shows the relative real permittivity ($\varepsilon'_{r,obs}$) and temperature coefficient of resonant frequency (τ_f) as a function of x value. The temperature-compensated mixture occurs near $x = 0.67$ with a corrected permittivity of ~ 32—the expected Qxf product (@7 GHz) is on the order of 10,000 GHz (Table 3); however, this value should be considered a minimum since the specimens were not fully dense, and those with $x < 1$ contained a small amount of $Ca_2Nb_2O_7$. The properties for pure Ca_2AlNbO_6 obtained here are similar to those reported by Kagata and Kato ($\varepsilon_r = 25$, $\tau_f = -87$ ppm/°C) (14), except for a higher Qxf product (14,000 vs 7500 GHz).

CaO:Nb_2O_5 System

The results obtained here for the binary system at calcia contents above 70 mol% are shown in Fig. 5. The perovskite derivative $Ca_4Nb_2O_9$ exhibited solid solution ranging from approximately 17 to 20.5 mol% Nb_2O_5. At $Ca_4Nb_2O_9$, the phase transition between the 2:1 and 1:1 ordered polymorphs (31, 32) was observed by X-ray diffraction to occur between specimens quenched from 1400 and 1450°C. For the specimens in the 2-phase region between the $Ca_4Nb_2O_9$ solid solution and CaO, the phase transition was found to occur at approximately 1375°C as shown in the phase diagram (Fig. 5). At 21 mol% Nb_2O_5, the metastable "3:1" (or "$LT_{1/4}$" (31, 32)) ordered polymorph of $Ca_4Nb_2O_9$ was found to be stable between 1375 and 1575°C.

TABLE 2

Sample Density (ρ), Observed and Corrected Dielectric Constants (ε_{obs} and ε_{corr}), and Corrected Temperature Coefficient of Permittivity (τ_ε) for Selected Compounds Found in the CaO–Al_2O_3–Nb_2O_5 System

Composition	ρ (%)	ε_{obs}	ε_{corr}	τ_ε (ppm/°C)
Ca_2AlNbO_6	93	25	27	170
$Ca_4Nb_2O_9$	84	28	36	19
$Ca_3Nb_2O_8$	82	37	50	−135
$Ca_2Nb_2O_7$	90	29	33	320
$CaNb_2O_6$	90	16	18	83
$CaAl_4O_7$	91	9	10	175
$Ca_3Al_2O_6$	93	14	15	776
$Ca_{12}Al_{14}O_{33}$	93	8	9	1644
$CaAl_2O_4$	90	8	10	124
$CaAl_{12}O_{19}$	76	10	15	−247
$AlNbO_4$	92	12	14	123

Note. Capacitance measurements, 1 MHz, 25°C.

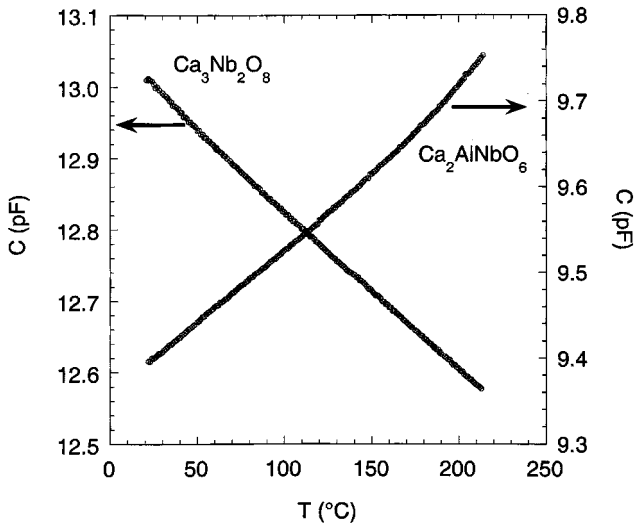

FIG. 3. Capacitance as a function of temperature for $Ca_3Nb_2O_8$ and Ca_2AlNbO_6. The temperature coefficients are opposite in sign and similar in magnitude.

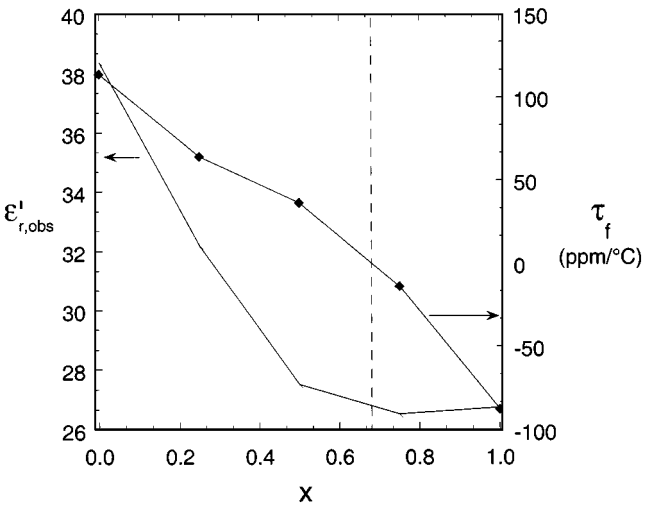

FIG. 4. Relative real permittivity ($\varepsilon'_{r,obs}$) and temperature coefficient of resonant frequency (τ_f) as a function of x value for xCa_2AlNbO_6:$(1-x)Ca_3Nb_2O_8$ compositions (Table 3). The temperature-compensated mixture occurs near $x = 0.67$ with a corrected permittivity of ~ 32.

Interestingly, the phase referred to as $Ca_3Nb_2O_8$ was found to occur with little or no solid solution at the composition 75.25:24.75 $CaO:Nb_2O_5$—stoichiometric specimens at $Ca_3Nb_2O_8$ (= 75:25 $CaO:Nb_2O_5$) always exhibited a small amount of $Ca_2Nb_2O_7$ in the X-ray powder diffraction patterns, despite repeated annealing at 1450°C. Closely spaced specimens were prepared in order to determine the composition at which "$Ca_3Nb_2O_8$" occurs as a single phase. As shown in Fig. 6, compositions on either side of 75.25:24.75 $CaO:Nb_2O_5$ exhibit traces of the expected neighboring binary phases. The $Ca_3Nb_2O_8$-type phase begins to decompose above 1475°C; thus, previously reported X-ray diffraction patterns of specimens annealed at higher temperatures show the presence of other phases. For example, in the pattern published for $Ca_3Nb_2O_{8-x}$, with indices based on a primitive tetragonal unit cell ($a = 16.90$, $c = 23.73$ Å, $P4/nnc$) (33), the peak indexed as (008) at $d = 2.9664$ Å in fact belongs to the impurity phase $Ca_2Nb_2O_7$. Assuming a perovskite-type structural formula $A_3B_3O_9$, with B-cation sites and oxygen sites fully occupied, $Ca_3Nb_2O_8$ corresponds to $Ca_{2.625}\square_{0.375}[Ca_{0.75}Nb_{2.25}]O_9$, where "□" denotes A-cation vacancies. Likewise, the single-phase composition 75.25:24.75 $CaO:Nb_2O_5$ corresponds to $Ca_{2.642}\square_{0.358}[Ca_{0.761}Nb_{2.239}]O_9$, which results

TABLE 3
Dielectric Properties of xCa_2AlNbO_6:$(1-x)Ca_3Nb_2O_8$ Mixtures[a]

x	ρ %	$\varepsilon'_{r,obs}$	$\varepsilon'_{r,corr}$	f (GHz)	τ_f (ppm/°C)	tan δ	Qxf (GHz)
0.000	88	38	45	5.8886	+113	8.3×10^{-4}	7100
0.250	87	32	40	6.3387	+64	8.5×10^{-4}	7500
0.500	83	28	36	6.8567	+36	7.7×10^{-4}	8900
0.750	88	26	32	6.9750	−14	5.3×10^{-4}	13,200
1.000	93	27	30	7.0163	−88	5.0×10^{-4}	14,000

Note. Dielectric resonator measurements, 30°C.

[a]The compound $Ca_3Nb_2O_8$ was later found to occur as a single phase at the compositioin 75.25:24.75 $CaO:Nb_2O_5$; therefore, the xCa_2AlNbO_6:$(1-x)Ca_3Nb_2O_8$ specimens with $x < 1$ actually contain from 1 to 4 mol% $Ca_2Nb_2O_7$, respectively, as a third phase. The dielectric properties obtained for single-phase "$Ca_3Nb_2O_8$" at 75.25:24.75 $CaO:Nb_2O_5$ are $\rho = 90\%$, $\varepsilon'_{r,obs} = 35$, $\varepsilon'_{r,corr} = 41$, $f = 8.6583$ GHz, $\tau_f = +123$ ppm/°C, tan $\delta = 1.0\times10^{-3}$, $Qxf = 8700$ GHz.

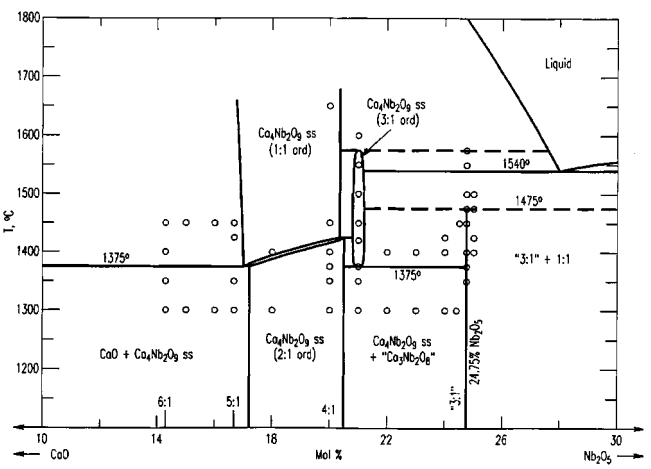

FIG. 5. Phase equilibria relations found in the CaO-rich portion of the $CaO:Nb_2O_5$ system. The "3:1" ordered polymorph of $Ca_4Nb_2O_9$, described elsewhere as the metastable "$LT_{1/4}$" phase (31, 32), was found to be stable at 21 mol% Nb_2O_5 between 1375 and 1575°C. The phase referred to as $Ca_3Nb_2O_8$ (= 75:25 $CaO:Nb_2O_5$) was found to occur with little or no solid solution at the composition 75.25:24.75 $CaO:Nb_2O_5$.

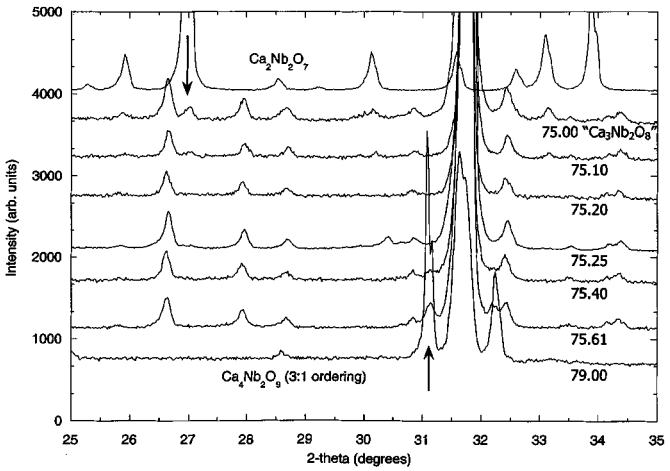

FIG. 6. X-ray diffraction patterns of $CaO:Nb_2O_5$ specimens near the composition $Ca_3Nb_2O_8$ (= 75:25 $CaO:Nb_2O_5$), which always exhibited small amounts of the neighboring binary compound $Ca_2Nb_2O_7$, as shown, despite extensive reannealing just below its decomposition temperature of 1475°C. The patterns are labeled according to mol% CaO. The compound referred to as $Ca_3Nb_2O_8$ was found to form as a single phase at 75.25:24.75 $CaO:Nb_2O_5$, as seen here. At CaO levels above 75.25 mol%, traces of the other neighboring compound $Ca_4Nb_2O_9$ appear in the X-ray powder diffraction pattern.

in a reduced number of cation vacancies; however, the reason that this compound forms at this particular stoichiometry is not known.

The X-ray powder diffraction data for the pure $Ca_3Nb_2O_8$-type phase (75.25:24.75 $CaO:Nb_2O_5$) up to $2\theta = 70^\circ$ could be completely indexed using a face-centered cubic cell with $a = 23.93$ Å. Single-crystal X-ray precession patterns with superstructure spots showing six times the basic 4-Å perovskite unit cell were also consistent with this cubic unit cell. However, optical microscopy indicated that the crystals were weakly birefringent rather than isotropic, and showed no sign of twinning. Examination of the high-angle ($2\theta > 70^\circ$) reflections in the X-ray powder diffraction data revealed that several strong peaks are split, indicating deviation from cubic symmetry. This peak splitting was especially noted for $(h^2 + k^2 + l^2)_{(\text{cubic})}$ sums equal to 432, 648, 720, and 864, as shown in Fig. 7. Further characterization of this phase using synchotron diffraction, neutron powder diffraction, electron diffraction, and single-crystal methods is in progress and will be described elsewhere.

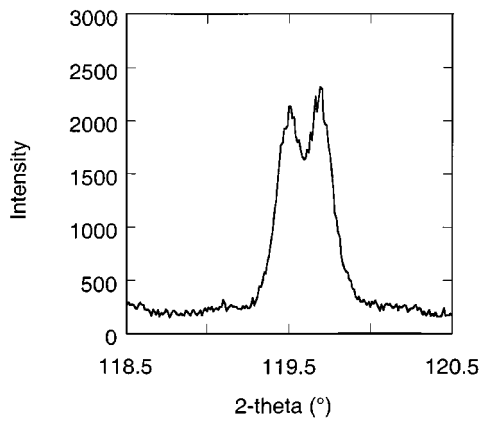

FIG. 7. High-angle, high-resolution X-ray powder diffraction pattern of the composition $75.25CaO:24.75Nb_2O_5$, which contains the $Ca_3Nb_2O_8$-type compound as a single phase, showing splitting of the diffraction peak $(h^2 + k^2 + l^2)_{(\text{cubic})} = 720$. The data shown were obtained with an incident beam monochromator and a PSD detector; therefore, $K\alpha_2$ lines are not present. This splitting indicates that the structure deviates from cubic symmetry. The detailed crystal structure of the $Ca_3Nb_2O_8$-type phase and the reason it occurs off-stoichiometry at $75.25CaO:24.75Nb_2O_5$, as essentially a point compound, are not yet known.

CONCLUSIONS

A subsolidus phase equilibria study of the $CaO:Al_2O_3:Nb_2O_5$ system at 1325°C in air indicates the occurrence of a single ternary compound, Ca_2AlNbO_6, that exhibits a perovskite-related structure with 1:1 or NaCl-type ordering of Al^{3+} and Nb^{5+} on the *B* sites. The X-ray powder diffraction pattern of this compound was indexed with a monoclinic unit cell ($P2_1/n$ (No. 11); $a = 5.3780(1)$, $b = 5.4154(1)$, $c = 7.6248(2)$ Å, $\beta = 89.968(2)^\circ$). Capacitance methods at 1 MHz were used to determine the dielectric constant and its temperature coefficient for 11 compounds in the system; the results suggested that a stable, temperature-compensated mixture could be prepared along the Ca_2AlNbO_6–$Ca_3Nb_2O_8$ composition line. Dielectric resonator methods at 5–7 GHz were used to determine the properties of 5 compositions in the xCa_2AlNbO_6:$(1 - x)$ $Ca_3Nb_2O_8$ system; temperature compensation of the resonant frequency was obtained near $x = 0.67$ with a permittivity of 32. No solid solution between Ca_2AlNbO_6 and $Ca_3Nb_2O_8$ was observed. The system CaO–Nb_2O_5 was reexamined at CaO contents above 70 mol% to clarify conflicting information in the literature. Two phases were confirmed to form in this region: the polymorphic-ordered perovskite $Ca_4Nb_2O_9$, with solid solution ranging from approximately 17 to 20.5 mol% Nb_2O_5, and the compound referred to as $Ca_3Nb_2O_8$, which was shown here to occur as essentially a point compound at the composition 75.25:24.75 $CaO:Nb_2O_5$. Structural characterization indicated that this phase is a defect perovskite with a noncubic unit cell; however, the detailed crystal structure and the reason it forms at this particular stoichiometry are not yet known.

ACKNOWLEDGMENTS

The authors appreciate helpful discussions with I. Levin. W. Febo was supported by the National Science Foundation Research Experience for Undergraduates (REU) program in the Division of Materials Research.

REFERENCES

1. W. Wersing, *in* "Electronic Ceramics" (B. C. H. Steele, Ed.), Chap. 4. Elsevier, New York, 1991.
2. W. Wersing, *Curr. Opin. Solid State Mater. Sci.* **1,** 715–731 (1996).
3. H. Sreemoolanadhan and M. T. Sebastian, *Metals Mater. Proc.* **7,** 251 (1995).
4. T. Negas, G. Yeager, S. Bell, and R. Amren, *in* "NIST Special Publication 804" (P. K. Davies and R. S. Roth, Eds.), pp. 21–38. NIST, 1991.
5. P. K. Davies, *in* "Materials and Processes for Wireless Communications" (T. Negas and H. Ling, Eds.), pp. 137–151. Amer. Ceram. Soc. Westerville, OH, 1995.
6. S. Kawashima, M. Nishida, I. Ueda, and H. Ouchi, *J. Am. Ceram. Soc.* **66,** 421–423 (1983).
7. S. B. Desu and J. M. O'Bryan, *J. Am. Ceram. Soc.* **68,** 546–551 (1983).
8. L. Chai and P. K. Davies, *J. Am. Ceram. Soc.* **80,** 3193 (1997), and references cited therein.
9. J. Y. Chan, I. Levin, T. A. Vanderah, R. G. Geyer, and R. S. Roth, *Intl. J. Inorg. Mater.* **2,** 107–114 (2000).
10. R. D. Shannon, *J. Appl. Phys.* **73,** 348–366 (1993).
11. E. L. Colla and N. Setter, *Mater. Res. Soc. Symp. Proc.* **453,** 437–442 (1997).
12. M. J. Geselbracht, "Probing Relative Acidities in Solid-Acid-Layered Perovskites," Contribution 269 at the 54th Northwest Regional Meeting of the American Chemical Society, Portland, OR, June 22, 1999.
13. K. Endo, K. Fujimoto, and K. Murakawa, *J. Am. Ceram. Soc.* **70,** C215–C218 (1987).
14. H. Kagata and J. Kato, *Jpn. J. Appl. Phys.* **33,** 5463–5465 (1994).
15. *Phase Equilibria Diagrams* (formerly *Phase Diagrams for Ceramists*). The American Ceramic Society, Westerville, OH. $CaO–Al_2O_3$: Figs. **1**:231, **2**:2295, **3**:4308, **4**:5141. $Al_2O_3–Nb_2O_5$: **2**:2349, **3**:4379, **4**:5191, **6**:6453. $CaO–Nb_2O_5$: **1**:244, **3**:4315.
16. A. K. Chatterjee and G. I. Zhmoidin, *J. Mater. Sci.* **7,** 93 (1972).
17. B. F. Pedersen, *Acta Chem. Scan.* **16,** 421 (1962).
18. N. F. Fedorov, I. F. Andreev, R. M. Kasparyan, and T. P. Smorodina, *Izv Akad Nauk SSSR Neorg. Mater.* **7,** 643 (1971).
19. R. Norin, *Acta Chem. Scan.* **23,** 1210 (1969).
20. A. D. Wadsley, *Acta Crystallogr.* **14,** 664–670 (1961).
21. R. S. Roth, A. D. Wadsley, and B. M. Gatehouse, *Naturwissenschaft* **51,** 262 (1964).
22. A. D. Wadsley and S. Andersson, *in* "Perspectives in Structural Chemistry" (J. D. Dunitz and J. A. Ibers, Eds.), Vol. 3, pp. 1–58. Wiley, New York, 1970.
23. M. Ibrahim, N. F. Bright, and J. F. Rowland, *J. Am. Ceram. Soc.* **45,** 329 (1962).
24. A. Jongejan, *J. Less Common Metals* **19,** 193 (1969).
25. J. K. Brandon and H. D. Megaw, *Philos. Mag.* **21,** 189 (1970).
26. K. Scheunemann and H. Müller-Buschbaum, *J. Inorg. Nucl. Chem.* **36,** 1965 (1974).
27. N. Ishizawa, F. Marumo, S. Iwai, M. Kimura, and T. Kawamura, *Acta Crystallogr. Sect. B* **36,** 763 (1980).
28. H. D. Hess and H. J. Trumpour, *Am. Miner.* **44,** 1 (1959).
29. J. F. Rowland, N. F. H. Bright, and A. Jonejan, *Adv. X-Ray Anal.* **2,** 97 (1960).
30. J. P. Cummings and S. H. Simonsen, *Am. Miner.* **55,** 90 (1970).
31. I. Levin, L. A. Bendersky, J. P. Cline, R. S. Roth, and T. A. Vanderah, *J. Solid State Chem.* **150,** 43 (2000).
32. I. Levin, J. Y. Chan, R. G. Geyer, J. E. Maslar, and T. A. Vanderah, *J. Solid State Chem.*, in pesss.
33. M. Hervieu, F. Studer, and B. Raveau, *J. Solid State Chem.* **22,** 273 (1977).
34. V. A. Filip'ev and E. G. Fesenko, *Sov. Phys. Crystallogr.* **10,** 243–247 (1965).
35. C. D. Brandle and V. J. Fratello, *J. Mater. Res.* **5,** 2160–2164 (1990).
36. I. Levin, J. Y. Chan, T. A. Vanderah, J. E. Maslar, and S. M. Bell, to be submitted.
37. C. R. Hubbard, Y. Zhang, and R. L. McKenzie, Certificate of Analysis, SRM 660, National Institute of Standards and Technology, Gaithersburg, MD (1989).
38. C. K. Lowe-Ma, Program CELLSVD, Naval Air Warfare Center Weapons Division Technical Publication 8128, 1993.
39. A. C. Larson and R. B. Von Dreele, GSAS—General Structure Analysis System, 1994.
40. A. H. Scott and H. L. Curtis, *J. Res. Natl. Bur. Stand.* **22,** 747 (1939).
41. D. A. G. Bruggeman, *Ann. Phys.* **24,** 636 (1935).
42. B. W. Hakki and P. D. Coleman, *IEEE Trans. Microwave Theory Tech.* **8,** 402–410 (1960).
43. W. E. Courtney, *IEEE Trans. Microwave Theory Tech.* **18,** 476–485 (1970).
44. J. Krupka, R. G. Geyer, and D. Cros, *in* "Proc. MIKON 94 Conf.," Vol. 2, pp. 567–572, 1994.
45. R. G. Geyer, J. Krupka, and C. Jones, *in* "Advances in Dielectric Ceramic Materials," pp. 75–91. Am. Ceram. Soc., Westerville, OH, 1998.
46. R. G. Geyer and J. Baker-Jarvis, "Effective Medium Theory for Ferrite-loaded Materials," NIST Tech. Note 1371, 1994.
47. R. G. Geyer, T. Vanderah, J. Baker-Jarvis, and J. Mantese, *in* "Advances in Dielectric Ceramic Materials," pp. 115–128. Am. Ceram. Soc., Westerville, OH, 1998.
48. G. S. Smith and R. L. Snyder, *J. Appl. Crystallogr.* **12,** 60 (1979).
49. T. A. Vanderah, T. R. Lindsey, and R. S. Roth, in preparation.
50. P. Rolando and G. Borroni Grassi, *Atti Accad. Sci. Torino Cl. Sci. Fis., Mat. Nat.* **110,** 371–378 (1976).